NOMA Receiver Design for Delay-Sensitive Systems

Tasneem Assaf, *Student Member, IEEE*, Arafat Al-Dweik, *Senior Member, IEEE*, Mohamed S. El Moursi, *Senior Member, IEEE*, Hatem Zeineldin, *Senior Member, IEEE*, and Mohammad Al-Jarrah, *Member, IEEE*

***Abstract*—Successive interference cancelation (SIC) has been considered widely for the detection of downlink nonorthogonal multiple access (NOMA) signals. However, the sequential detection inherent to SIC process may introduce additional time delay for certain users, making the SIC unsuitable for communication systems with time delay constraints such as wireless networks that utilize unmanned aerial vehicles or low earth orbit satellites. Therefore, this article considers the performance of NOMA systems using a joint multiuser detector (JMuD), which can detect the signals of all users simultaneously and, hence, reduce the detection time requirements. The performance of the JMuD is evaluated in terms of bit error rate (BER), computational complexity, and processing time and compared to the SIC detector (SICD). The exact BER of the JMuD is derived analytically using quadrature phase shift keying modulation where closed-form expressions are derived for the two- and three-user scenarios for the air-to-ground channel, which is modeled as a Rician fading channels with order statistics. The obtained analytical results corroborated by Monte Carlo simulation confirm that the BERs of the JMuD and SICD are identical; however, the processing time of the SICD is 51% more than the JMuD for several cases of interest.**

***Index Terms*—Bit error rate (BER), joint detection, maximum likelihood detection (MLD), nonorthogonal multiple access (NOMA), successive interference cancelation (SIC).**

I. Introduction

THE utilization of unmanned aerial vehicles (UAVs) and small low Earth orbit satellites (LEOSs), such as CubeSat, for various applications has witnessed a significant increase in the last few years. Moreover, UAVs and LEOSs are expected to be part of future wireless networks [1]–[3], which is part of the emerging concept of flying networks. In flying network applications, the communicating devices are expected to download or relay a massive amount of information in short time periods that are upper bounded by the flyover time, which is typically very short. Furthermore, the timing window for data transfer might be even limited to the channel coherence time, which is much shorter than the flyover time. This is required to avoid extensive channel-state-information (CSI) exchange and, hence, reducing the signaling overhead [4]. Although the downlink data rate is generally determined by the transmitter, it is not actually the case when the network protocol supports handshaking to provide reliable data communications [5]. In such scenarios, the average data rate is determined by both, the transmitter and receiver, and if the receiver's response to the handshaking request is slow, the average data rate may drop significantly [6], [7]. Consequently, such systems should be equipped with highly efficient transmitter and receiver designs to satisfy such stringent timing constraints.

Nonorthogonal multiple access (NOMA) is an efficient multiple access technique, which is considered as a promising candidate for future wireless communication networks [8]–[20]. NOMA can improve the spectral efficiency by allowing multiple users to share the transmission resources simultaneously at the expense of some additional receiver complexity and bit error rate (BER) degradation [21]. Several NOMA schemes have been proposed in the literature, but the main categories are the code [14], [22] and power NOMA [23], [24], which is the focus of this article.

The basic concept of power NOMA is that multiple users may share transmission resources simultaneously by assigning each user a particular power [25]. In the literature, successive interference cancelation (SIC) has been considered widely [9], [11], [13], [14], [16]–[18], [26]–[28] as the main detection scheme for NOMA signals. However, SIC detectors (SICDs) suffer from long processing times because the nth user has to sequentially detect, modulate, and subtract the signals of users 1, 2,. . ., $n-1$ [29]. To reduce the processing time, joint multiuser detection (JMuD) has been proposed as an alternative for the SICD [29]–[33].

The BER analysis of NOMA using SICD has received extensive attention in the recent literature [9], [14], [18], [34], [35]. Nevertheless, to the best of the authors' knowledge, the exact BER of NOMA using JMuD has never been derived. Moreover, the computational complexity for the three-user NOMA and the processing time of the JMuD has never been compared to the SICD. Therefore, unlike the work of [33] which presents an upper bound on the BER and compares the complexity of the SICD and JMuD for the two-user scenario, the aim of this article is to derive the exact BER of NOMA systems using JMuD, evaluate its computational time and complexity, and compare them to the SICD for the two- and three-user scenarios. Such comparison enables the system designer to optimize the system

Manuscript received May 23, 2020; revised September 19, 2020; accepted October 18, 2020. Date of publication November 9, 2020; date of current version December 9, 2021. This work was supported by Khalifa University under the flagship project entitled "MUSES: Multiuse Space Energy Systems" under Grant 8474000026. The work of Arafat Al-Dweik was supported by the KU Center for Cyber-Physical Systems under Grant C2PS-T2. *(Corresponding author: Arafat Al-Dweik.)*

Tasneem Assaf and Mohamed S. El Moursi are with the Department of Electrical Engineering and Computer Science, Khalifa University, Abu Dhabi 127788, United Arab Emirates (e-mail: tasneem.assaf@ku.ac.ae; mohamed.elmoursi@ku.ac.ae).

Arafat Al-Dweik is with the Department of Electrical Engineering and Computer Science, Center for Cyber Physical Systems, Khalifa University, Abu Dhabi 127788, UAE, and also with the Department of Electrical and Computer Engineering, Western University, London, ON N6A 3K7, Canada (e-mail: dweik@fulbrightmail.org).

Hatem Zeineldin is with the Faculty of Engineering, Cairo University, Giza 12613, Egypt, and also with the Khalifa University, Abu Dhabi 127788, UAE (e-mail: hatem.zeineldin@ku.ac.ae).

Mohammad Al-Jarrah is with the School of Electrical and Electronic Engineering, University of Manchester, M13 9PL Manchester, U.K. (e-mail: mohammad.al-jarrah@manchester.ac.uk).

Digital Object Identifier 10.1109/JSYST.2020.3032878

configuration to satisfy time and complexity constraints. The obtained analytical and simulation results show that the BERs of the JMuD and SICD are identical, while the processing time and complexity are drastically different. More specifically, the processing time of the JMuD is substantially less than the SICD because it can perform the detection process for any user without waiting for other users' signal to be detected, modulated, and subtracted. On the contrary, the complexity of the JMuD is generally higher than the SICD because the transmitted signal constellation size increases exponentially with the number of users, while it increases linearly in the case of SICD. Moreover, the SICD structure depends on the relative power of each user; hence, receiver reconfiguration is required every time the power coefficients change their order, which may introduce additional delay and hardware complexity. Such a problem does not exist in the JMuD; however, all users should use maximum likelihood detection (MLD) while considering the superimposed constellation.

The rest of the article is organized as follows. In Section II, the system and channel models are presented. The exact BER analysis for the two- and three-user NOMA systems are presented in Sections III and IV, respectively. The complexity comparison between SICD and JMuD is represented in Section VI , while numerical and simulation results are shown in Section VII. Finally, the article is concluded in Section VIII.

II. System and Channel Models

This article considers power-domain downlink NOMA systems with N users, $U_1, ..., U_N$, where the users' equipment (UE) and the base station (BS) are equipped with a single antenna [9]. Consequently, the multiuser signal transmitted from the BS can be described as

$$x = \sum_{n=1}^{N} \sqrt{\beta_n P_T} s_n \tag{1}$$

where s_n is the data symbol of the nth user that is selected uniformly from a Gray coded quadrature-phase shift keying (QPSK) symbol constellation, P_T is the BS total transmit power, and β_n is the allocated power coefficient for the nth user. For the rest of the article, the transmit power P_T is normalized to unity, and, thus, $\sum_{n=1}^{N} \beta_n = 1$. For notation simplicity, we define $s_n = a_k \rightarrow s_n^{(k)}$, $k \in \{0, 1, 2, 3\}$, $a_0 = 00$, $a_1 = 01$, $a_2 = 10$, and $a_3 = 11$. For the case of QPSK and for $N \leq 3$, the in-phase $x_I \triangleq \Re(x)$ and quadrature $x_Q \triangleq \Im(x)$ components for each constellation point of the superimposed symbol x can be defined as

$$A_{u_1 u_2 u_3} = \sum_{i=1}^{3} u_i \sqrt{\beta_i},\ u_i \in \{0, 1, \acute{1}, 2\} \tag{2}$$

where $\acute{1} \triangleq -1$. For example, given that $s_1^{(2)} = s_2^{(2)}$, then $x = 1010$ and $x_I = -\sqrt{\beta_1} - \sqrt{\beta_2} \triangleq A_{\acute{1}\acute{1}0}$, and $x_Q = \sqrt{\beta_1} + \sqrt{\beta_2} \triangleq A_{110}$. It should be noted that u_3 represents the amplitude of the third user in $N = 3$ NOMA system.

An example for the case is shown in Fig. 1, where the two users use QPSK. The most left and right two bits belong to the first and second users, respectively. As can be noted from the figure, the constellation of the NOMA symbol x looks like a 16 quadrature amplitude modulation (QAM) constellation. In flat fading channels, the received signal at the nth UE can be expressed as

$$r_n = h_n x + w_n \tag{3}$$

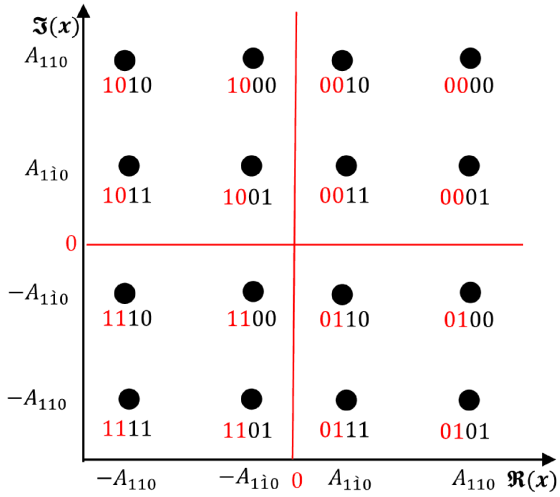

Fig. 1. Constellation diagram of the transmitted symbol x for $N = 2$.

where h_n represents the complex channel frequency response between the BS and nth user, the channel envelope $|h_n| \triangleq \alpha_n$, and w_n is the additive white Gaussian noise (AWGN), $w_n \sim \mathcal{CN}(0, 2\sigma_w^2)$. In NOMA systems, it is typically assumed that the first user has the lowest channel gain, the second user has the second lowest channel gain, and so forth, i.e., $\alpha_1 < \alpha_2 < \cdots < \alpha_N$. Thus, the power coefficients should be allocated in the opposite order of the channel gains, i.e., $\beta_1 > \beta_2 > \cdots > \beta_N$. The channel coefficients considered in this article follow the air-to-ground (AG) model presented in [36] and [37]. The extensive measurements in [36] and [37] show that the AG link can be modeled as a frequency-selective Rician fading channel with a K factor that ranges from 2 to 20 dB. The channel ordering is assumed to remain fixed for the coherence time of the channel, which can be more than 5 ms [38], which allows a reasonable CSI exchange frequency.

For coherent detection, the channel phase $\arg\{h_n\} \triangleq \theta_n$ can be estimated and compensated separately from α_n. Given that the channel phase θ_n is estimated and compensated perfectly at the nth UE receiver, then the received signal after phase compensation can be written as

$$\check{r}_n = r_n e^{-j\theta_n} = \alpha_n x + \check{w}_n \tag{4}$$

where $\check{w}_n = w_n e^{-j\theta_n}$. Assuming that w_n is circularly symmetric, then $\check{w}_n \sim w_n \sim \mathcal{CN}(0, 2\sigma_w^2)$. To extract the information symbols $s_n\ \forall n$, two possible detectors can be utilized, the SICD and JMuD. The JMuD is similar to the MLD used with QAM signals, except that the bits in each symbol belong to multiple users.

A. Detection of NOMA Signals Using JMuD

Based on the constellation diagram of Fig. 1, the JMuD of the nth user can be written as

$$\{\hat{s}_1, \hat{s}_2, \ ..., \hat{s}_N\} = \arg \min_{\tilde{s}_1, \tilde{s}_2, ..., \tilde{s}_N} \left| r_n - \hat{h}_n \sum_{i=1}^{N} \sqrt{\beta_i} \tilde{s}_i \right|^2 \tag{5}$$

where $\tilde{s}_i$ are the trial values of s_i and $\hat{h}_n$ is the estimated value of h_n. By noting that the modulation order of the superimposed symbol is $M_1 \times M_2 \times \cdots \times M_N$, the complexity of the detector increases exponentially as a function of the number of users. However, it is interesting to note that to detect the symbols of the nth user, the JMuD can be designed such that

the constellation size is $M_1 \times M_2 \times \cdots \times M_n$, and, hence, the detector will be similar to (5) except that N is replaced by n. Therefore, the signals of users $\{n+1, n+2, \ldots, M\}$ can be considered as unknown additive noise. For example, the first user detector can be written as

$$\hat{s}_1 = \arg\min_{\tilde{s}_1} \left| r_1 - \hat{h}_1 \sqrt{\beta_1} \tilde{s}_1 \right|^2 \tag{6}$$

which is the typical MLD for QPSK signals. It is straightforward to show that the BERs of the two detectors in (5) and (6) are identical, and, thus, it is preferable complexity-wise to use the MLD in (6).

B. Detection of NOMA Signals Using SICD

The NOMA signals can also be detected using the SICD approach, where the signal for the nth user is detected after detecting and subtracting the signals of the first $n-1$ users. Therefore, MLD is applied n times; however, the constellation size in each round is equal to the modulation order of the nth user signal, and, thus

$$\hat{s}_n = \arg\min_{\tilde{s}_n} \left| r_n - \hat{h}_n \sum_{i=1}^{n-1} \sqrt{\beta_i} \hat{s}_i - \hat{h}_n \sqrt{\beta_n} \tilde{s}_n \right|^2. \tag{7}$$

For the first user, it is clear that both the MLD (6) and SICD (7) have the same structure and, hence, the same BER, which is given in [9]. Moreover, it is worth noting the similarity between the SICD and JMuD in the sense that the signals of U_1, ..., U_{n-1} are involved in the detection of the signal of U_n.

III. JMuD BER Analysis $(U_1|_{N=2}, U_2|_{N=2})$

This section considers a two-user NOMA system using QPSK modulation. The transmitted superimposed symbol x is the superposition of two QPSK symbols, and, hence, it corresponds to 1 out of 16 constellation points each of which has 4 b, as shown in Fig. 1. The bit representation for each point is expressed as b_{ni}, $\{n, i\} \in \{1, 2\}$, where n is the user index and i is the bit index.

For the first user, the detection is performed using (6). Based on the specific value of s_1 and the interuser interference (IUI) caused by U_2, symbol x may become one of the four constellation points in the neighborhood of s_1 shown in Fig. 1.

The average BER should consider all possible combinations of s_1 and s_2

$$P_{b_{1i}} = \sum_{l,k} \left(P_{b_{1i}}|_{s_1^{(l)}, s_2^{(k)}} \right) \mathrm{P}\left(s_1^{(l)}, s_2^{(k)} \right). \tag{8}$$

It should be noted that s_1 and s_2 are independent, then (8) can be written as

$$P_{b_{1i}} = \frac{1}{16} \sum_{\{l.k\}=0}^{3} \left(P_{b_{1i}}|_{s_1^{(l)}, s_2^{(k)}} \right). \tag{9}$$

Case 1: $s_1^{(2)}$, $s_2^{(0)}$: The error probability of b_{11}, $P_{b_{11}}|_{s_1^{(2)}, s_2^{(0)}}$, depends only on the in-phase component of $\check{r}_1$, i.e., $\Re(\check{r}_1) \triangleq \mathfrak{r}_1$ and the specific value of x, $x = -A_{1\acute{1}0} + jA_{110}$. Thus

$$\begin{aligned} P_{b_{11}}|_{s_1^{(2)}, s_2^{(0)}} &= \mathrm{P}(\mathfrak{r}_1 \geq 0) \\ &= \mathrm{P}(-\alpha_1 A_{1\acute{1}0} + \mathfrak{n}_1 \geq 0) \\ &= \mathrm{P}(\mathfrak{n}_1 \geq \alpha_1 A_{1\acute{1}0}) \end{aligned} \tag{10}$$

where $\mathfrak{r}_1 = -\alpha_1 A_{1\acute{1}0} + \mathfrak{n}_1$, $\Re(\check{w}_1) \triangleq \mathfrak{n}_1$. Therefore

$$\begin{aligned} P_{b_{11}}|_{s_1^{(2)}, s_2^{(0)}} &= \frac{1}{\sqrt{2\pi\sigma_{\mathfrak{n}_1}^2}} \int_{\alpha_1 A_{1\acute{1}0}}^{\infty} e^{-\frac{z^2}{2\sigma_{\mathfrak{n}_1}^2}} d\mathfrak{n}_1 \\ &= Q\left(\sqrt{\gamma_{1,1}} \right) \end{aligned} \tag{11}$$

where $\gamma_{1,1} = \gamma \alpha_1^2 A_{1\acute{1}0}^2$, $\gamma = \frac{1}{\sigma_w^2}$, and $Q(.)$ denotes the Gaussian Q function.

Case 2: $s_1^{(2)}$, $s_2^{(1)}$: By following the same approach of *Case* 1, the error probability of this case is given by (11) as well.

Case 3: $s_1^{(2)}$, $s_2^{(2)}$: The error probability can be expressed as

$$\begin{aligned} P_{b_{11}}|_{s_1^{(2)}, s_2^{(2)}} &= \mathrm{P}(\mathfrak{r}_1 \geq 0) \\ &= \mathrm{P}(\mathfrak{n}_1 \geq \alpha_1 A_{110}). \end{aligned} \tag{12}$$

Following the same approach used to derive (11) gives

$$P_{b_{11}}|_{s_1^{(2)}, s_2^{(2)}} = Q\left(\sqrt{\gamma_{1,2}} \right) \tag{13}$$

where $\gamma_{1,2} = \gamma \alpha_1^2 A_{110}^2$.

Case 4: $s_1^{(2)}$, $s_2^{(3)}$: The probability of error in this case is similar to the case of $s_1^{(2)}$, $s_2^{(2)}$.

Cases 5–16 are evaluated using the same approach, except that the value of s_1 is replaced by a_0, a_1, a_2, and a_3. Through the substitution of the 16 cases results in (9), the conditional BER for the bit b_{11} can be expressed as

$$P_{b_{11}} = \frac{1}{2} \left[Q\left(\sqrt{\gamma_{1,1}} \right) + Q\left(\sqrt{\gamma_{1,2}} \right) \right]. \tag{14}$$

Clearly, $P_{b_{12}} = P_{b_{11}}$. Therefore, the conditional BER of the first user is given

$$\begin{aligned} P_{U_1} &= \frac{1}{2} \left[P_{b_{11}} + P_{b_{12}} \right] \\ &= \frac{1}{2} \left[Q\left(\sqrt{\gamma_{1,1}} \right) + Q\left(\sqrt{\gamma_{1,2}} \right) \right]. \end{aligned} \tag{15}$$

As for the second user, the JMuD requires a 16-point MLD as shown in (5).

The error probability for the second user can be computed by evaluating the error probability for each individual bit, i.e., b_{21} and b_{22}. Because the error probability depends on s_1 and s_2, then

$$P_{b_{2i}} = \sum_{l,v} \left(P_{b_{2i}}|_{s_1^{(l)}, s_2^{(v)}} \right) \mathrm{P}\left(s_1^{(l)}, s_2^{(v)} \right). \tag{16}$$

By noting that s_1 and s_2 are independent, then (16) for the 16-point constellation can be written as

$$P_{b_{2i}} = \frac{1}{16} \sum_{\{l,v\}=0}^{3} \left(P_{b_{2i}}|_{s_1^{(l)}, s_2^{(v)}} \right). \tag{17}$$

The following cases cover the error probability of all possible constellation points of x.

Case 1. $s_1^{(0)}$, $s_2^{(0)}$*:* For this case, the transmitted signal is $x = A_{110} + jA_{110}$ and an error occurs if $\hat{s}_1 = a_2$ (10) or a_3 (11). Consequently, the error probability of b_{21} can be expressed as

$$\begin{aligned} P_{b_{21}}|_{s_1^{(0)}, s_2^{(0)}} &= \mathrm{P}(\mathfrak{r}_2 \leq \alpha_2 A_{100}, \mathfrak{r}_2 \geq 0 \cup \mathfrak{r}_2 \leq \alpha_2 A_{\acute{1}00}) \\ &= \mathrm{P}(\mathfrak{r}_2 \leq \alpha_2 A_{100}, \mathfrak{r}_2 \geq 0) + \mathrm{P}(\mathfrak{r}_2 \leq \alpha_2 A_{\acute{1}00}) \\ &\quad - \mathrm{P}(\mathfrak{r}_2 \leq \alpha_2 A_{100}, \mathfrak{r}_2 \geq 0, \mathfrak{r}_2 \leq \alpha_2 A_{\acute{1}00}) \\ &= \mathrm{P}(\mathfrak{n}_2 \leq \alpha_2 A_{0\acute{1}0}) - \mathrm{P}(\mathfrak{n}_2 \leq \alpha_2 A_{\acute{1}\acute{1}0}) \\ &\quad + \mathrm{P}(\mathfrak{n}_2 \leq \alpha_2 A_{\acute{2}\acute{1}0}) \end{aligned} \tag{18}$$

where $\mathfrak{r}_2 \triangleq \Re(x) = \alpha_2 A_{110} + \mathfrak{n}_2$ and $\Re(\check{w}_2) \triangleq \mathfrak{n}_2$. By noting that

$$\begin{aligned}\mathrm{P}(\mathfrak{n}_2 \geq \alpha_2 A_{u_1u_2u_3}) &= \frac{1}{\sqrt{2\pi\sigma^2_{\mathfrak{n}_2}}} \int_{\alpha_2 A_{u_1u_2u_3}}^{\infty} e^{-\frac{z^2}{2\sigma^2_{\mathfrak{n}_2}}} d\mathfrak{n}_2 \\ &= Q\left(\sqrt{\gamma_{2,c}}\right) \end{aligned} \tag{19}$$

where $\gamma_{2,c} = \gamma\alpha_2^2 A^2_{u_1u_2u_3}$. Then

$$P_{b_{21}}|_{s_1^{(0)},\, s_2^{(0)}} = Q\left(\sqrt{\gamma_{2,1}}\right) - Q\left(\sqrt{\gamma_{2,2}}\right) + Q\left(\sqrt{\gamma_{2,3}}\right) \tag{20}$$

where $\gamma_{2,1} = \gamma\alpha_2^2 A^2_{010}$, $\gamma_{2,2} = \gamma\alpha_2^2 A^2_{110}$, and $\gamma_{2,3} = \gamma\alpha_2^2 A^2_{210}$. Following the same approach for all constellation points that correspond to the combinations $[s_1^{(0)}, s_2^{(1)}]$, $[s_1^{(1)}, s_2^{(0)}]$, and $[s_1^{(1)}, s_2^{(1)}]$ gives the same probability of error for $P_{b_{21}}|_{s_1^{(0)},\, s_2^{(0)}}$. Therefore, $P_{b_{21}}|_{s_1^{(0)},\, s_2^{(0)}} = P_{b_{21}}|_{s_1^{(0)},\, s_2^{(1)}} = P_{b_{21}}|_{s_1^{(1)},\, s_2^{(0)}} = P_{b_{21}}|_{s_1^{(1)},\, s_2^{(1)}}$, which is given by (20).

Case 2. $s_1^{(0)}, s_2^{(2)}$*:* For this case $x = A_{1\acute{1}0} + jA_{110}$. The error probability of b_{21} can be obtained as

$$\begin{aligned} P_{b_{21}}|_{s_1^{(0)},\, s_2^{(2)}} &= \mathrm{P}(\mathfrak{r}_2 \geq \alpha_2 A_{100} \cup \mathfrak{r}_2 \geq \alpha_2 A_{\acute{1}00}, \mathfrak{r}_2 \leq 0) \\ &= \mathrm{P}(\mathfrak{r}_2 \geq \alpha_2 A_{100}) + \mathrm{P}(\mathfrak{r}_2 \geq \alpha_2 A_{\acute{1}00}, \mathfrak{r}_2 \leq 0) \\ &\quad - \mathrm{P}(\mathfrak{r}_2 \geq \alpha_2 A_{100}, \mathfrak{r}_2 \geq \alpha_2 A_{\acute{1}00}, \mathfrak{r}_2 \leq 0) \\ &= \mathrm{P}(\mathfrak{n}_2 \geq \alpha_2 A_{010}) \\ &\quad + \mathrm{P}(\mathfrak{n}_2 \geq \alpha_2 A_{\acute{2}10}, \mathfrak{n}_2 \leq \alpha_2 A_{\acute{1}10}) \\ &= \mathrm{P}(\mathfrak{n}_2 \geq \alpha_2 A_{010}) \\ &\quad + \mathrm{P}(\alpha_2 A_{\acute{2}10} \leq \mathfrak{n}_2 \leq \alpha_2 A_{\acute{1}10}) \\ &= Q\left(\sqrt{\gamma_{2,1}}\right) + Q\left(\sqrt{\gamma_{2,4}}\right) - Q\left(\sqrt{\gamma_{2,5}}\right) \end{aligned} \tag{21}$$

where $\gamma_{2,4} = \gamma\alpha_2^2 A^2_{1\acute{1}0}$ and $\gamma_{2,5} = \gamma\alpha_2^2 A^2_{2\acute{1}0}$. It can be noted that the constellation points that correspond to the combinations $[s_1^{(0)}, s_2^{(3)}]$, $[s_1^{(1)}, s_2^{(2)}]$ and $[s_1^{(1)}, s_2^{(3)}]$ have the same probability, which is given by (21).

Case 3. $s_1^{(2)}, s_2^{(0)}$*:* For this case, $x = -A_{1\acute{1}0} + jA_{110}$, and then the error probability can be expressed as

$$\begin{aligned} P_{b_{21}}|_{s_1^{(2)},\, s_2^{(0)}} &= \mathrm{P}(\mathfrak{r}_2 \leq \alpha_2 A_{\acute{1}00} \cup \mathfrak{r}_2 \leq \alpha_2 A_{100}, \mathfrak{r}_2 \geq 0) \\ &= \mathrm{P}(\mathfrak{r}_2 \leq \alpha_2 A_{\acute{1}00}) + \mathrm{P}(\mathfrak{r}_2 \leq \alpha_2 A_{100}, \mathfrak{r}_2 \geq 0) \\ &\quad - \mathrm{P}(\mathfrak{r}_2 \leq \alpha_2 A_{\acute{1}00}, \mathfrak{r}_2 \leq \alpha_2 A_{100}, \mathfrak{r}_2 \geq 0) \\ &= \mathrm{P}(\mathfrak{n}_2 \leq \alpha_2 A_{0\acute{1}0}) + \mathrm{P}(\mathfrak{n}_2 \leq \alpha_2 A_{2\acute{1}0}) \\ &\quad - \mathrm{P}(\mathfrak{n}_2 \leq \alpha_2 A_{1\acute{1}0}) \\ &= Q\left(\sqrt{\gamma_{2,1}}\right) + Q\left(\sqrt{\gamma_{2,4}}\right) - Q\left(\sqrt{\gamma_{2,5}}\right). \end{aligned} \tag{22}$$

The same error probability in (22) is also applicable for the combinations $[s_1^{(2)}, s_2^{(1)}]$, $[s_1^{(3)}, s_2^{(0)}]$, and $[s_1^{(3)}, s_2^{(1)}]$.

Case 4. $s_1^{(2)}, s_2^{(2)}$*:* For this case, $x = -A_{110} + jA_{110}$, and the error probability can be expressed as

$$\begin{aligned} P_{b_{21}}|_{s_1^{(2)},\, s_2^{(2)}} &= \mathrm{P}(\mathfrak{r}_2 \geq \alpha_2 A_{\acute{1}00}, \mathfrak{r}_2 \leq 0 \cup \mathfrak{r}_2 \geq \alpha_2 A_{100}) \\ &= Q\left(\sqrt{\gamma_{2,1}}\right) - Q\left(\sqrt{\gamma_{2,2}}\right) + Q\left(\sqrt{\gamma_{2,3}}\right). \end{aligned} \tag{23}$$

The result in (23) is also applicable to the combinations $[s_1^{(2)}, s_2^{(3)}]$, $[s_1^{(3)}, s_2^{(2)}]$, and $[s_1^{(3)}, s_2^{(3)}]$.

Finally, substituting (20)–(23) into (17) gives the unconditional error probability of b_{21}. Moreover, by following the same approach for b_{22}, it can be shown that $P_{22} = P_{21}$. Consequently, the error probability for the second user can be expressed as

$$P_{U_2} = \frac{1}{2}\sum_{i=1}^{5} v_i Q\left(\sqrt{\gamma_{2,i}}\right), \mathbf{v} = [2, -1, 1, 1, -1]. \tag{24}$$

Interestingly, P_{U_1} and P_{U_2} are actually equal to [9, Eq. 12 and 36], respectively, which implies that the BERs of the JMuD and SICD are identical. Nevertheless, the analysis for the JMuD is much simpler because it does not require considering the impact of the SICD process on users 1,2, $3, \ldots, n-1$. The average BERs over ordered Rician flat fading channels, $\bar{P}_{U_1}$ and $\bar{P}_{U_2}$, are evaluated by averaging over the probability density function (PDF) of $\gamma_{n,i}$ as shown in Appendix.

IV. JMuD BER Analysis ($U_2|_{N=3}, U_3|_{N=3}$)

In this section, the BER derivation of $N = 3$ downlink NOMA system is illustrated. The transmitted symbol x forms a 64-point constellation as shown in [9], and the first, second, and third users' signals are given by s_1, s_2, and s_3, respectively. The binary bit representation for the three users is given by $\begin{bmatrix} b_{11} & b_{12} & b_{21} & b_{22} & b_{31} & b_{32} \end{bmatrix}$, for each bit b_{ni}, $n = \{1, 2, 3\}$, and $i = \{1, 2\}$. Similar to $N = 2$ scenario, the derivation of the first user BER is the same for both JMuD and SICD [9] because MLD given in (6) is used for QPSK constellation.

For the second user, the BER is evaluated as follows. The probability of error for each bit depends on the values of s_1 and s_2, and, hence, the average BER should consider all possible combinations. Nevertheless, due to space limitations, and because the solution procedure is similar for all cases, we consider only the case of $[s_1^{(0)}, s_2^{(0)}, s_3^{(0)}]$. For this case, $x = A_{111} + jA_{111}$ and b_{21} can be expressed as

$$\begin{aligned} P_{b_{21}}|_{s_1^{(0)}, s_2^{(0)}} &= \mathrm{P}(\mathfrak{r}_2 \leq \alpha_2 A_{100}, \mathfrak{r}_2 \geq 0 \cup \mathfrak{r}_2 \leq \alpha_2 A_{\acute{1}00}) \\ &= \mathrm{P}(\alpha_2 A_{\acute{1}\acute{1}\acute{1}} \leq \mathfrak{n}_2 \leq \alpha_2 A_{0\acute{1}\acute{1}}) + \mathrm{P}(\mathfrak{n}_2 \leq \alpha_2 A_{\acute{2}\acute{1}\acute{1}}) \\ &= Q\left(\sqrt{\gamma_{3,5}}\right) - Q\left(\sqrt{\gamma_{3,4}}\right) + Q\left(\sqrt{\gamma_{3,10}}\right) \end{aligned} \tag{25}$$

$$\begin{aligned} P_{b_{31}}|_{s_1^{(0)}, s_2^{(0)}, s_3^{(0)}} &= \mathrm{P}(\mathfrak{r}_3 \leq \alpha_3 A_{110}, \mathfrak{r}_3 \geq \alpha_3 A_{100} \cup \mathfrak{r}_3 \leq \alpha_3 A_{1\acute{1}0}, \mathfrak{r}_3 \geq 0 \cup \mathfrak{r}_3 \leq -\alpha_3 A_{1\acute{1}0}, \mathfrak{r}_3 \geq \alpha_3 A_{\acute{1}00} \cup \mathfrak{r}_3 \leq -A_{110}) \\ &= \mathrm{P}(\mathfrak{n}_3 \leq \alpha_3 A_{00\acute{1}}, \mathfrak{n}_3 \geq \alpha_3 A_{0\acute{1}\acute{1}}) + \mathrm{P}(\alpha_3 A_{111} + \mathfrak{n}_3 \leq \alpha_3 A_{1\acute{1}0}, \alpha_3 A_{111} + \mathfrak{n}_3 \geq 0) + \mathrm{P}(\alpha_3 A_{111} + \mathfrak{n}_3 \leq -A_{110}) \\ &\quad + \mathrm{P}(\alpha_3 A_{111} + \mathfrak{n}_3 \leq -\alpha_3 A_{1\acute{1}0}, \alpha_3 A_{111} + \mathfrak{n}_3 \geq \alpha_3 A_{\acute{1}00}) \\ &= \mathrm{P}(\mathfrak{n}_3 \leq \alpha_3 A_{00\acute{1}}) - \mathrm{P}(\mathfrak{n}_3 \leq \alpha_3 A_{0\acute{1}\acute{1}}) + \mathrm{P}(\mathfrak{n}_3 \leq \alpha_3 A_{0\acute{2}\acute{1}}) - \mathrm{P}(\mathfrak{n}_3 \leq \alpha_3 A_{\acute{1}\acute{1}\acute{1}}) + \mathrm{P}(\mathfrak{n}_3 \leq \alpha_3 A_{\acute{2}0\acute{1}}) \\ &\quad - \mathrm{P}(\mathfrak{n}_3 \leq \alpha_3 A_{\acute{2}\acute{1}\acute{1}}) + \mathrm{P}(\mathfrak{n}_3 \leq \alpha_3 A_{\acute{2}\acute{2}\acute{1}}) \\ &= -Q\left(\sqrt{\gamma_{3,4}}\right) - Q\left(\sqrt{\gamma_{3,5}}\right) - Q\left(\sqrt{\gamma_{3,10}}\right) + Q\left(\sqrt{\gamma_{3,11}}\right) + Q\left(\sqrt{\gamma_{3,12}}\right) + Q\left(\sqrt{\gamma_{3,13}}\right) + Q\left(\sqrt{\gamma_{3,18}}\right) \end{aligned} \tag{26}$$

where $\gamma_{3,4}$, $\gamma_{3,5}$, and $\gamma_{3,10}$ are defined in [9]. By following the same approach used in Section III, the exact BER for both b_{21} and b_{22} can be evaluated for all possible combinations of s_1, s_2, which interestingly show that the JMuD and SICD have equal BERs.

For $U_3|_{N=3}$, the JMuD adopts a 64-point MLD constellation. Similar to the previous cases, the error probability depends on s_1, s_2, and s_3. Nevertheless, because the solution procedure is similar for all cases, we only consider the case of $[s_1^{(0)}, s_2^{(0)}, s_3^{(0)}]$. For this case, $P_{b_{31}}$ can be expressed as shown in (26) at the bottom of the previous page, where the terms $\gamma_{3,4}$, $\gamma_{3,5}$, $\gamma_{3,10}$, $\gamma_{3,11}$, $\gamma_{3,12}$, $\gamma_{3,13}$, and $\gamma_{3,18}$ are defined in [9].

It is worth noting that deriving analytical BER expressions for NOMA using arbitrary number of users N and modulation orders M_1, M_2, ..., M_N is highly desirable. However, such a task requires an entirely dedicated work as reported in [39], where the BER is derived for an arbitrary M_n, but the results are limited for the two-user scenario, i.e., $N = 2$.

V. Power Allocation

The power allocation (PA) problem is formulated to minimize the overall average BER of the NOMA system while ensuring fairness for all users. Fairness is defined as maintaining a specific BER thresholds for each user. Therefore, the problem can be formulated as

$$\min_{\ddot{\beta}_n} \frac{1}{N} \sum_{n=1}^{N} \bar{P}_{U_n} \tag{27a}$$

subject to

$$\sum_{n=1}^{N} \beta_n = 1 \tag{27b}$$

$$\bar{P}_{U_n} \leq \bar{P}_{U_n}^{\text{th}} \forall n \in \{1, 2, \ldots, N\} \tag{27c}$$

$$\beta_l \geqslant \beta_k, l \neq k, l < k, \{l, k\} \in \{1, 2, \ldots, N\} \tag{27d}$$

where $\ddot{\beta}_n$ and $\bar{P}_{U_n}^{\text{th}}$ are the optimal power coefficient and BER threshold for the nth user, respectively. Constraint (27b) is used to assure that the total transmit power is limited to unity. Constraint (27c) is used to assure that each user's BER is less than its desired threshold, and (27d) forces the power allocated for each user to be inversely proportional to its channel gain, i.e., $\beta_1 > \beta_2 > \cdots > \beta_N$ are assigned for the users with the channel gains $\alpha_1 < \alpha_2 < \cdots < \alpha_N$, respectively. The problem in (27a) is a constrained nonlinear optimization problem which is analytically intractable. Hence, numerical methods such as brute-force and bisection [7] can be used to search for the near-optimum power coefficients. It should be noted that the difference from the optimal solution depends on the search step size.

VI. JMuD and SICD Complexity

Although the JMuD and SICD have the same BER performance, their receivers' structure are fundamentally different, and, hence, the complexity for each detector should be evaluated and compared. The complexity comparison in this article will be conducted by evaluating the computational time and hardware complexity. The computational complexity is evaluated in terms of the number of real arithmetic operations required to evaluate the detectors described in (5) and (7), where $N = 2$ and 3, and all users adopt QPSK modulation. For more informative comparison, the overall equivalent complexity is also presented [40] as depicted in Table I. As can be noted from the table, the computational complexity of the JMuD is considerably higher than the SICD due to the large number of multiplications associated with the MLD. Moreover, the JMuD complexity increases exponentially by increasing the user index because the modulation order of the symbol to be detected increases also exponentially as a function of its index. Thus, the complexity depends on the user index rather than the total number of users.

TABLE I
Computational Complexity of the JMuD and SICD

	Operation	SICD	JMuD	Ratio %
$U_2\|_{N=2}$	$\times$	53	176	
	$\pm$	70	176	
Overall Equivalent Complexity		282	880	32.0
$U_2\|_{N=3}$	$\times$	53	176	
	$\pm$	70	176	
Overall Equivalent Complexity		282	880	32.0
$U_3\|_{N=3}$	$\times$	82	704	
	$\pm$	108	704	
Overall Equivalent Complexity		436	3520	12.3

The time complexity corresponds to the latency of receiver, which is defined as the time required to produce the final hard bits from the received signal. Generally speaking, the MLD can perform the detection process for all users simultaneously, and all the Euclidean distance measurements can be performed in parallel. For the SICD, the detection process per user is performed sequentially, i.e., first user, then second user, etc. Moreover, the detected bits of each user has to be re-encoded and re-modulated to be subtracted from the superimposed signal. As a result, the time complexity of the SICD is expected to be more than the JMuD. The results presented in Section VII show that the simulation time required by the SICD is about 86% as compared to the JMuD in certain scenarios. Therefore, the JMuD is more suitable for time sensitive applications.

The hardware complexity of the JMuD is similar to a conventional M-ary QAM MLD. For the SICD, the receiver should also implement part of the transmitter chain for the SIC process. Therefore, the SICD should consist of an encoder and modulator, in addition to the MLD. Although most devices are built as transceivers, using the transmitter subsystem in the detection process is mostly infeasible as most systems support full-duplex operations. Therefore, the detector should have dedicated encoders and modulators. It is also worth noting that the SICD has to be reconfigured when the power order of the users is changed, which may introduce additional delay and hardware complexity. Such a problem does not exist in the JMuD.

VII. Numerical Results

This section presents the analytical and Monte Carlo simulation results for the JMuD and SICD over Rician channel. Two-user and three-user NOMA downlink systems are considered, $N = 2$ and $N = 3$. All users are assumed to be equipped with a single antenna, and the channel between the BS and each user is modeled as an ordered Rician flat fading channel. The randomly generated channels are ordered based on their strength, where the weakest channel is assigned to U_1 and the strongest channel is assigned to U_N. The transmitted symbols for all users are selected uniformly from a Gray coded QPSK constellation. The

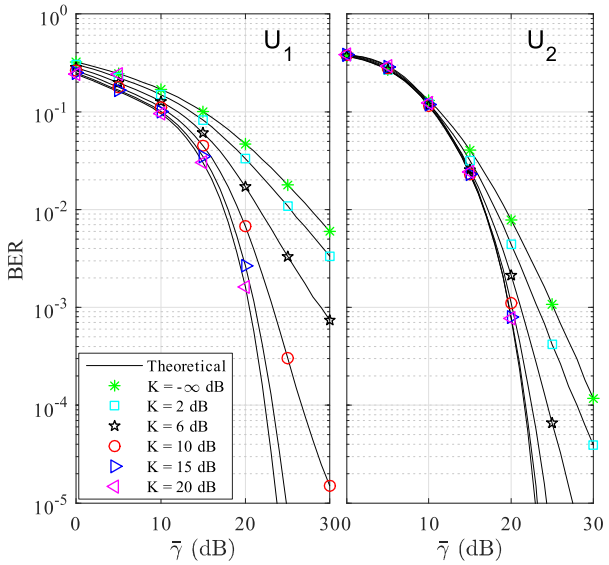

Fig. 2. Average BER for the U_1 and U_2, where $K = [-\infty, 2, 6, 10, 15, 20]$ dB, $\beta_1 = 0.7$, and $\beta_2 = 0.3$.

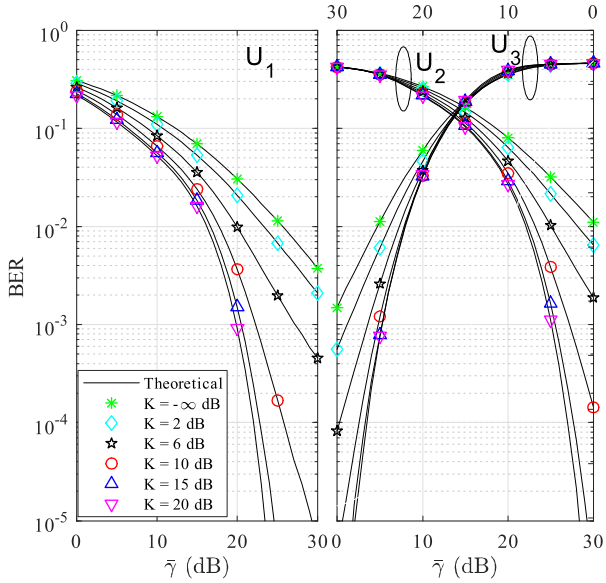

Fig. 3. Average BER for the U_1, U_2, and U_3, where $K = [-\infty, 2, 6, 10, 15, 20]$ dB, $\beta_1 = 0.8$, $\beta_2 = 0.15$, and $\beta_3 = 0.05$.

total transmit power from the BS is unified for all cases, $P_T = 1$. The simulation results are obtained using a computing machine that runs Intel Xeon CPU E5-2640 processor, clock frequency of 2.5 GHz, 16 GB RAM, and 64 b operating system.

Fig. 2 presents the analytical and simulation BER performance for power coefficients $\beta_1 = 0.7$ and $\beta_2 = 0.3$ and various values of K over a range of $\bar{\gamma}$, where $\bar{\gamma} = \frac{1}{\sigma_w^2}$. As can be noted from the figure, the analytical results obtained using (44) and (52) perfectly match the simulation results for all the considered values of K and $\bar{\gamma}$. It is worth noting that the Rayleigh fading case corresponds to $K = -\infty$ dB. As can be seen from the figure, the performance of the first user is more sensitive to the variations of K as compared to the second user, which is due to the fact that the fading effect becomes less significant for the near users.

Fig. 3 shows the BER for $N = 3$ using various K values. As can be noted from the figure, U_3 has generally the best performance although it is allocated the smallest power coefficient. Such performance is obtained because U_3 has the best channel as compared to U_1 and U_2. Similar to the two-user NOMA system, the error performance of the first user is more sensitive to the value of K if compared to the second and third users. This is due to the fact that the fading effect becomes less significant for the near users.

Although the BER expressions in (45) are represented in terms of infinite series, the series can be truncated to have $\{G, M\}$ and $\{G, M, Z\}$ finite terms, for the first and second users, respectively. In order to ensure numerical accuracy, the values of G, M, and Z are selected based on the system parameters, such as the fading parameter K and $\bar{\gamma}$. For simplicity, it is assumed that $G = M$ and $G = M = Z$, for the first and second users, respectively. Tables II and III show the normalized truncation error for the average BER expressions of U_1 and U_2. The normalized truncation error is computed as follows:

$$e_t = \frac{|\text{BER}_{\text{Sim}} - \text{BER}_{\text{Theo}}|}{\text{BER}_{\text{Sim}}} \tag{28}$$

where the BER_{Theo} and BER_{Sim} are the analytical and simulated BERs, respectively. The depicted results show that when

TABLE II
NORMALIZED TRUNCATION ERROR FOR $\bar{\gamma} = 10$ AND 20 dB AND $K = 6$ dB FOR THE FIRST USER

$\{G, M\}$	e_t, $\bar{\gamma} = 10$ dB	$\{G, M\}$	e_t, $\bar{\gamma} = 20$ dB
5	0.4636	5	0.2470
10	3.76×10^{-2}	10	2.7×10^{-3}
30	6.3955×10^{-4}	30	1.5×10^{-3}
50	6.3955×10^{-4}	50	1.5×10^{-3}

TABLE III
NORMALIZED TRUNCATION ERROR FOR $\bar{\gamma} = 10$ AND 20 dB AND $K = 6$ dB FOR THE SECOND USER

$\{G, M, Z\}$	e_t, $\bar{\gamma} = 10$ dB	$\{G, M, Z\}$,	e_t, $\bar{\gamma} = 20$ dB
5	0.4913	5	2.2748
10	5.61×10^{-2}	10	4.11×10^{-2}
30	1.5777×10^{-4}	30	2.3×10^{-3}
50	1.5777×10^{-4}	50	2.3×10^{-3}

$\{G, M\} = 30$, the truncation error is fairly insignificant for different $\bar{\gamma}$ values and $K = 6$ dB.

Fig. 4 shows the effect of K on the BER of each user for $N = 2$ with $\bar{\gamma} = 16$ and 18 dB. The PA coefficients are $\beta_1 = 0.7$ and $\beta_2 = 0.3$. As can be noted from the figure, the BER is highly dependent on K, particularly for U_1 who experiences more severe fading conditions. Consequently, its BER is more sensitive to the values of K. Moreover, the BER for both users becomes more sensitive to K as $\bar{\gamma}$ increases, which is due to the fact that the channel fading effect becomes more dominant at high SNRs. It is also worth noting from the figure that the BER of U_2 does not necessarily decrease when K increases. For example, Fig. 4, where $\bar{\gamma} = 18$ dB, shows that the BER keeps decreasing until $K = 15$ dB and then increases again until it saturates when the AWGN and IUI have more impact on the BER. Such behavior can be justified using the envelop of the received signal PDFs given in Fig. 5, which represents the conditional PDF for the received signal of the second user at $\bar{\gamma} = 10$ dB and $K = 8$ and 10 dB. Clearly, the two PDFs have the same mean, but the standard deviation for the case of $K = 8$ dB is lower. It should be noted that as $K \to \infty$, the BER will be

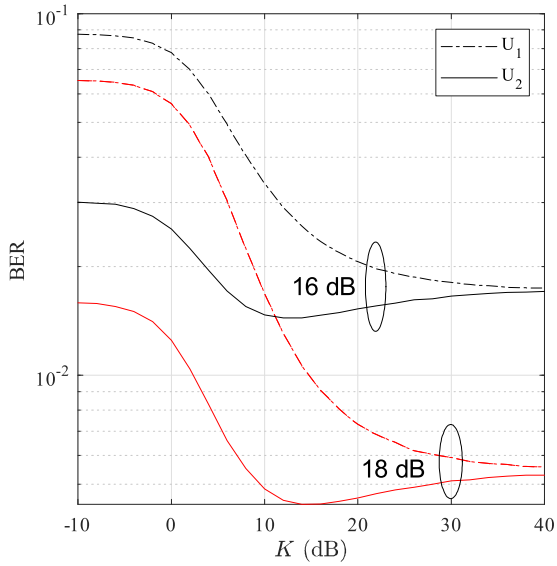

Fig. 4. Average BER for the first and second users under Rician channel, where $\bar{\gamma} = 16$ and 18 dB.

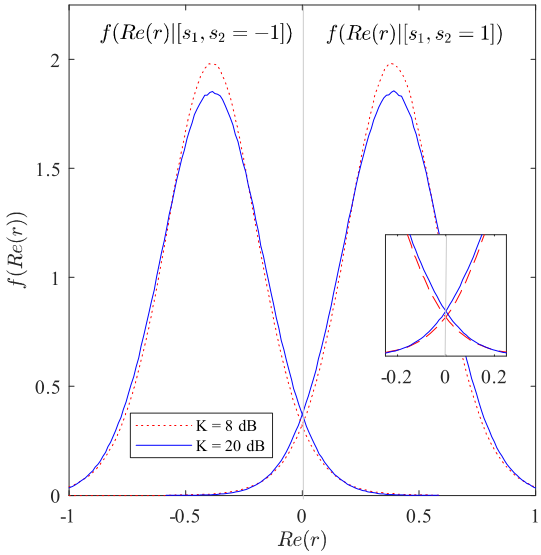

Fig. 5. Conditional PDF for the received signal of the second user at $\bar{\gamma} = 10$ dB.

TABLE IV
POWER ALLOCATION TO ACHIEVE MINIMUM AVERAGE BER, $K = 2, 6$ AND 15 dB

	$K = 2$ dB		$K = 6$ dB		$K = 15$ dB	
$\bar{\gamma}$ dB	β_1	β_2	β_1	β_2	β_1	β_2
10	-	-	-	-	-	-
20	-	-	0.86	0.14	0.83	0.17
30	0.95	0.05	0.94	0.06	0.92	0.08

mostly determined the IUI, the power coefficients, and AWGN. For the power coefficients considered in Fig. 4, the BER of both users converge roughly to the same value.

Table IV presents the optimal power coefficients that minimize the BER for different values of $\bar{\gamma}$, for $K = 2$,6 and 15 dB, and for BER thresholds of $\bar{P}_{U_1}^{\text{th}} = 10^{-2}$ and $\bar{P}_{U_2}^{\text{th}} = 10^{-3}$. The power coefficients are obtained using brute-force with a step size of 0.01. As can be noted from the table, the BER constraint could not be satisfied for $\bar{\gamma} = 10$ dB regardless of the value of K, and for $K = 2$ dB when $\bar{\gamma} = 20$ dB. The results also show

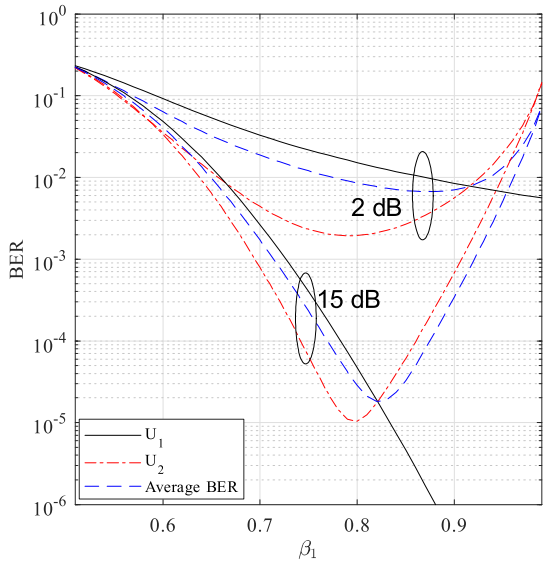

Fig. 6. Average BER for the first and second users over different power allocation coefficients, $K = 2$ and 15 dB and $E_b/N_0 = 20$ dB.

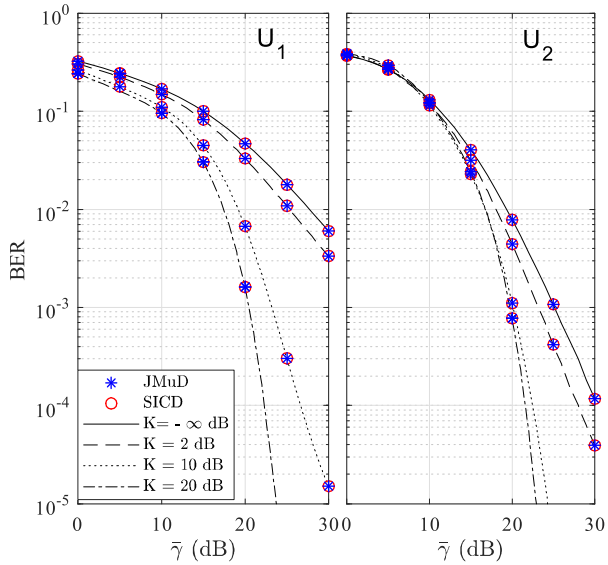

Fig. 7. Average BER comparison between JMuD and SICD under Rician channels for the U_1 and U_2 users, where $K = [-\infty, 2, 10, 20]$ dB.

that most of the power is allocated for U_1, particularly at high $\bar{\gamma}$. The first user is allocated more than 95% of the total power at $\bar{\gamma} = 30$ dB and $K = 2$ dB. The same trends can be noted for the $K = 6$ and 15 dB cases. Nevertheless, the power given to the U_1 generally decreases by increasing K.

Fig. 6 shows the average BER for the two users and system average BER over a range of β_1 values at $\bar{\gamma} = 20$ dB and $K = 2$, and 6 dB. At $K = 2$ dB, minimum average BER cannot be found for $\bar{P}_{U_1}^{\text{th}} = 10^{-2}$ and $\bar{P}_{U_2}^{\text{th}} = 10^{-3}$. As for the other scenario where $K = 15$ dB, the power coefficients are $\beta_1 = 0.82$ and $\beta_1 = 0.18$.

Fig. 7 shows the BER performance for the two users in $N = 2$ downlink NOMA system using JMuD and SICD [9]. As can be noted, both detectors result in identical BER performance over the entire $\bar{\gamma}$ range and K values.

To evaluate the impact of the sequential detection on the delay of the SICD, the simulation time for the SICD T_{SICD}

TABLE V
COMPUTATIONAL TIME IN MILLISECONDS

	T_{SICD}	T_{JMuD}	Δ_T (%)
$U_1\|_{N=2}$	12	12	0.0
$U_2\|_{N=2}$	52	29	79.3
$U_1\|_{N=3}$	20	20	0.0
$U_2\|_{N=3}$	41	22	86.3
$U_3\|_{N=3}$	68	45	51.1

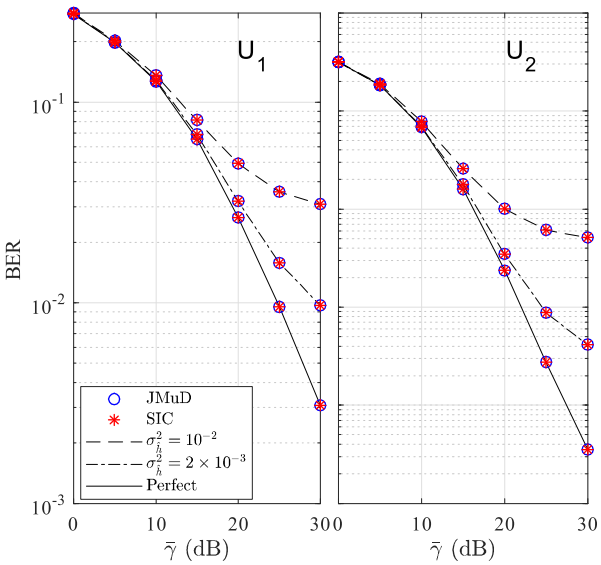

Fig. 8. Average BER for $N = 2$ downlink NOMA system with JMuD and SICD with perfect channel estimation, imperfect channel estimation, $\beta_1 = 0.7$, and $\sigma_{\hat{h}}^2 = 10^{-2}$ and 2×10^{-3}.

is measured for a total of 10^6 symbols and compared to the JMuD simulation time T_{JMuD}. Table V presents T_{SICD} and T_{JMuD} in milliseconds and also shows the normalized difference Δ_T between the two detectors, $\Delta_T \triangleq |T_{\text{SICD}} - T_{\text{JMuD}}|/T_{\text{JMuD}}$. As can be noted from Table V, the SICD requires significant extra time due to the sequential detection process. It is also worth noting that the simulation time for the JMuD also increases by increasing the user order due to the additional computational complexity caused by the increased constellation order that the JMuD has to detect. As expected, the simulation time for the first user is independent of N and the detector type.

Fig. 8 shows the average BER for $N = 2$ with imperfect channel estimates. The channel estimation errors are modeled as $\mathcal{CN}(0, \sigma_{\hat{h}}^2)$ [41], [42] , where $\sigma_{\hat{h}}^2 = 1 \times 10^{-2}$ and 2×10^{-3}. As can be noted, both detectors perform equivalently under channel estimation errors, and both detectors are highly sensitive to estimation errors.

Fig. 9 presents the BER for the first and second users in $N = 2$ system using JMuD under Rician and Nakagami-m channels. Every value of K corresponds to an m value, where the relation is as follows [43]:

$$m = \frac{\bar{K}^2}{1 + 2K} \tag{29}$$

where $K + 1 \triangleq \bar{K}$. Clearly, as K increases, the BER results under the two distributions become closer. For the considered scenario, the BER of the two channels completely matched when $K = 17$ dB and $m = 14.1182$ dB. It should be noted that for large values of K, the Rician distribution can be approximated by the Nakagami-m distribution.

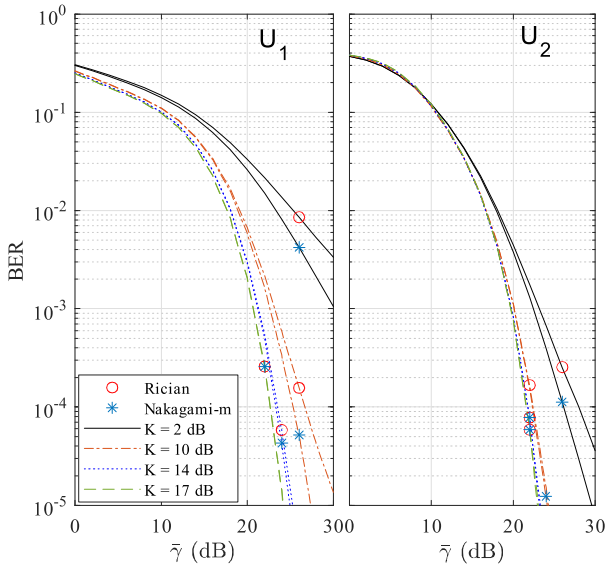

Fig. 9. Average BER for the first and second users under Rician and the equivalent Nakagami-m fading channels, where $K = 2$, 10, 14, and 17 dB.

TABLE VI
THEORETICAL AND NUMERICAL DIVERSITY FOR $N = 2$ NOMA SYSTEM, $K = [-\infty, 2, 6]$ dB

K dB	D_1 (30)	$\tilde{D}_1$	Δ_1	D_2(30)	$\tilde{D}_1$	Δ_2
$-\infty$	1	0.998	0.002	2.0	1.99	0.005
2	1.6024	1.490	0.069	3.204	3.11	0.0274
6	2.7684	2.653	0.041	5.880	5.676	0.0244

The diversity gain can be defined as $D_n \triangleq \lim_{\bar{\gamma}\to\infty} \frac{\log \bar{P}_{U_n}}{\log \bar{\gamma}}$, which is intractable for the Rician channel due to the hypergeometric and Bessel functions. Therefore, an approximated D_n can be derived by approximating the Rician PDF by the Nakagami-m distribution. Consequently, using the BER expression for NOMA in Nakagami-m channels [9, Eq. (101)] and considering only the dominant components, the diversity gain can be given as

$$D_n \approx -\lim_{\bar{\gamma}\to\infty} \frac{\log\left(\frac{1}{\bar{\gamma}}\right)^{mn}}{\log \bar{\gamma}} \approx mn. \tag{30}$$

Table VI shows the diversity gain for $N = 2$ and $K = [-\infty, 2, 6]$ dB obtained from (30) compared to another approximation obtained from the BER curves denoted as $\tilde{D}_n$, which is the BER slope at high $\bar{\gamma}$ values. As can be noted from the table, the normalized difference $\Delta_n \triangleq |D_n - \tilde{D}_n|/D_n$. As can be indicated from (30), the diversity gain of the nth user converges to mn. Moreover, the normalized difference Δ_n is fairly small for all the considered cases.

VIII. CONCLUSION AND FUTURE WORK

This article presented the BER analysis of the JMuD for downlink NOMA systems where a closed-form analytical expressions are derived for several cases of interest. Moreover, the work presented a general comparison for the JMuD and the widely adopted SICD. The comparison is performed in terms of BER, computational complexity, processing time, and sensitivity to channel estimation errors. Although the two detectors are fundamentally different, the obtained analytical and simulation results show that both detectors have identical BERs in the case of perfect and imperfect channel estimates, yet the

derivation is significantly different. The BER analysis for the JMuD requires considering much smaller number of cases and, hence, can be considered much simpler than the SICD BER analysis. The BER sensitivity to channel estimation errors was evaluated using Monte Carlo simulation for both systems, and the obtained results show that both systems have equivalent sensitivity. The computational complexity results show that the SICD has much lower complexity as compared to the JMuD but at the expense of a longer processing time. Therefore, the JMuD would be preferable for cases where the processing delay is paramount while the SICD would be preferable in all other cases.

As can be noted from this article and the listed references, the exact BER derivation for an arbitrary number of users and modulations schemes remains an open problem that will be considered in our future work. Moreover, the analysis will be extended to the case where the phase for each user can be modified to improve the system performance.

APPENDIX
AVERAGE BER OVER RICIAN FADING CHANNEL

As described in Section II, the channel between the UAV and ground follows the Rician distribution; thus, the envelops of the channels $\alpha_n \, \forall n \in N$ are ordered set of Rician random variables. Using the theory of order statistics, the PDF for each channel can be expressed as [44, pp. 225]

$$f_n(\alpha) = K_n f(\alpha) [F(\alpha)]^{n-1} [1 - F(\alpha)]^{N-n} \tag{31}$$

where $K_n = \frac{N!}{(n-1)!(N-n)!}$, α is the channel envelop which follows Rician distribution, and $f(\alpha)$ and $F(\alpha)$ are the PDF and cumulative distribution function (CDF) of α, respectively, which are given by

$$f(\alpha) = \frac{2\bar{K}\alpha}{\Omega} \mathrm{e}^{-\left(\frac{\bar{K}\alpha^2}{\Omega} + K\right)} I_0\left(\sqrt{\frac{4K\bar{K}\alpha^2}{\Omega}}\right) \tag{32}$$

and

$$F(\alpha) = 1 - Q_1\left(\sqrt{2K}, \sqrt{\frac{2K\alpha^2}{\Omega}}\right) \tag{33}$$

where K and Ω are the Rician distribution parameters, $K + 1 \triangleq \bar{K}$, $I_0(\cdot)$ is the modified Bessel function of the first kind, and $Q_1(\cdot, \cdot)$ is the Marcum-Q function. The infinite series representation of Q_1 can be represented as [45]

$$Q_1(x, y) = \mathrm{e}^{-\frac{x^2+y^2}{2}} \sum_{m=0}^{\infty} \left(\frac{x}{y}\right)^m I_m(xy). \tag{34}$$

Therefore, the general ordered PDF of the nth channel envelope over Rician channel is

$$f_n(\alpha) = \frac{2\bar{K}K_n\alpha}{\Omega \mathrm{e}^{\left(\frac{\bar{K}\alpha^2}{\Omega} + K\right)}} \left[1 - Q_1\left(\sqrt{2K}, \sqrt{\frac{2\bar{K}}{\Omega\alpha^{-2}}}\right)\right]^{n-1} \times \left[Q_1\left(\sqrt{2K}, \sqrt{\frac{2\bar{K}\alpha^2}{\Omega}}\right)\right]^{N-n} I_0\left(\sqrt{\frac{4K\bar{K}\alpha^2}{\Omega}}\right).$$

In order to avoid confusion, let us denote $f_n(\alpha) \to f_n(\alpha_n)$.

Now, γ follows the noncentral chi-square χ^2 distribution with the following PDF and CDF [46]

$$f(\gamma) = \frac{\bar{K}\mathrm{e}^{-\left(K + \bar{K}\varpi\right)}}{\bar{\gamma}} I_0\left(\sqrt{4K\bar{K}\varpi}\right) \tag{35}$$

and

$$F(\gamma) = 1 - Q_1\left(\sqrt{2K}, \sqrt{2\bar{K}\varpi}\right) \tag{36}$$

where $\varpi = \frac{\gamma}{\bar{\gamma}}$. By using (31), the general ordered PDF for γ can be expressed as follows:

$$f_n(\gamma) = \frac{\bar{K}K_n\mathrm{e}^{-\left(K+\bar{K}\varpi\right)}}{\bar{\gamma}} I_0\left(\sqrt{4K\bar{K}\varpi}\right) \times \left[1 - \mathrm{e}^{-\left(K+\bar{K}\varpi\right)} \sum_{m=0}^{\infty} \left(\sqrt{\frac{K}{\bar{K}\varpi}}\right)^m I_m\left(\sqrt{4K\bar{K}\varpi}\right)\right]^{n-1} \times \left[\mathrm{e}^{-\left(K+\bar{K}\varpi\right)} \sum_{m=0}^{\infty} \left(\sqrt{\frac{K}{\bar{K}\varpi}}\right)^m I_m\left(\sqrt{4K\bar{K}\varpi}\right)\right]^{N-n}.$$

To avoid confusion, let $f_n(\gamma) \to f_n(\gamma_{n,i})$, where i is a parameter index. For simplicity, let $\eta_{n,i} = \frac{\bar{K}\mathrm{e}^{-K}}{\bar{\gamma}_{n,i}}$, $\epsilon_{n,i} = \frac{4K\bar{K}}{\bar{\gamma}_{n,i}}$, $\varphi = 2K$, and $\mu_{n,i} = \frac{2\bar{K}}{\bar{\gamma}_{n,i}}$.

Then, for the two-user NOMA system, the ordered PDFs for the first and second users $\gamma_{n,i}$, $n \in \{1, 2\}$, $N = 2$ can be, respectively, represented as

$$f_1(\gamma_{1,i}) = K_1\eta_{1,i}\mathrm{e}^{-\frac{\mu_{1,i}}{4}} I_0\left(\sqrt{\epsilon_{1,i}\gamma_{1,i}}\right) \mathrm{e}^{-\gamma_{1,i}\mu_{1,i}} \times \sum_{m=0}^{\infty} \left(\frac{\varphi}{\mu_{1,i}\gamma_{1,i}}\right)^{\frac{m}{2}} I_m\left(\sqrt{\epsilon_{1,i}\gamma_{1,i}}\right) \tag{37}$$

and

$$f_2(\gamma_{2,i}) = K_2\eta_{2,i}\mathrm{e}^{-\frac{\mu_{1,i}\gamma_{2,i}}{2}} I_0\left(\sqrt{\epsilon_{2,i}\gamma_{2,i}}\right) - K_2\eta_{2,i}\mathrm{e}^{-\frac{\varphi}{2}} I_0\left(\sqrt{\epsilon_{2,i}\gamma_{2,i}}\right) \mathrm{e}^{-\gamma_{2,i}\mu_{2,i}} \times \sum_{m=0}^{\infty} \left(\frac{\varphi}{\mu_{2,i}\gamma_{2,i}}\right)^{\frac{m}{2}} I_m\left(\sqrt{\epsilon_{2,i}\gamma_{2,i}}\right). \tag{38}$$

In order to evaluate the average BER of the two users in $N = 2$ system over Rician channel, (37) and (38) are utilized as follows:

$$\int_0^{\infty} Q\left(\sqrt{\gamma_{n,i}}\right) f_n(\gamma_{n,i}) \, d\gamma_{n,i}. \tag{39}$$

By using (15) and (37), the average BER for $n = 1$ can be computed as

$$\begin{aligned}\overline{P}_{U_1} &= \frac{1}{2} \sum_{i=1}^{2} \left[\int_0^{\infty} Q\left(\sqrt{\gamma_{1,i}}\right) f_1(\gamma_{1,i}) \, d\gamma_{1,i}\right] \\ &= \frac{K_1}{2} \sum_{i=1}^{2} \eta_{1,i}\mathrm{e}^{-\frac{\varphi}{2}} \int_0^{\infty} Q\left(\sqrt{\gamma_{1,i}}\right) \\ &\quad \times I_0\left(\sqrt{\epsilon_{1,i}\gamma_{1,i}}\right) \mathrm{e}^{-\gamma_{1,i}\mu_{1,i}} \\ &\quad \times \sum_{m=0}^{\infty} \left(\frac{\varphi}{\mu_{1,i}\gamma_{1,i}}\right)^{\frac{m}{2}} I_m\left(\sqrt{\epsilon_{1,i}\gamma_{1,i}}\right) d\gamma_{1,i}. \end{aligned} \tag{40}$$

By replacing the Q function by its alternative representation defined by [47], $Q(x) = \frac{1}{\pi}\int_0^{\frac{\pi}{2}} \mathrm{e}^{-\left(\frac{x^2}{2\sin^2(\phi)}\right)} d\phi$, and (40) becomes as in (41) shown at the top of next page, where $\xi_{n,i}(\varrho) = \frac{2\sin^2(\phi_{n,i})}{2\varrho\sin^2(\phi_{n,i})+1}$.

Evaluating the inner integral in (41) shown at the top of next page, gives the single integral expression given in (42), shown at the top of next page [45], where

$$\overline{P}_{U_1} = \frac{K_1 \mathrm{e}^{-\frac{\varphi}{2}}}{2\pi} \sum_{i=1}^{2} \left[\int_0^{\infty} \int_0^{\frac{\pi}{2}} \eta_{1,i} \mathrm{e}^{-\left(\frac{\gamma_{1,i}}{2\sin^2(\phi_{1,i})}\right)} d\phi_{1,i} I_0\left(\sqrt{\epsilon_{1,i}\gamma_{1,i}}\right) \mathrm{e}^{-\gamma_{1,i}\mu_{1,i}} \sum_{m=0}^{\infty} \left(\sqrt{\frac{\varphi}{\mu_{1,i}\gamma_{1,i}}}\right)^m I_m\left(\sqrt{\epsilon_{1,i}\gamma_{1,i}}\right) d\gamma_{1,i} \right]$$
$$= \frac{K_1 \mathrm{e}^{-\frac{\varphi}{2}}}{2\pi} \sum_{i=1}^{2} \left[\sum_{m=0}^{\infty} \eta_{1,i} \left(\frac{\varphi}{\mu_{1,i}}\right)^{\frac{m}{2}} \int_0^{\frac{\pi}{2}} \int_0^{\infty} \frac{1}{(\gamma_{1,i})^{\frac{m}{2}}} \mathrm{e}^{-\frac{\gamma_{1,i}}{\xi_{1,i}(\mu_{1,i})}} I_0\left(\sqrt{\epsilon_{1,i}\gamma_{1,i}}\right) I_m\left(\sqrt{\epsilon_{1,i}\gamma_{1,i}}\right) d\gamma_{1,i} d\phi_{1,i} \right] \tag{41}$$

$$\overline{P}_{U_1} = \frac{K_1 \mathrm{e}^{-\frac{\varphi}{2}}}{2\pi} \sum_{i=1}^{2} \left[\sum_{m=0}^{\infty} \frac{\eta_{1,i}\xi_{1,i}\left(\mu_{1,i}\right)\left(\frac{\varphi\epsilon_{1,i}}{4\mu_{1,i}}\right)^{\frac{m}{2}}}{\Gamma(m+1)} {}_2F_1\left(1+\frac{m}{2}, \frac{m}{2}+\frac{1}{2}; m+1, m+1; \epsilon_{1,i}\xi_{1,i}\left(\mu_{1,i}\right)\right) d\phi_{1,i} \right] \tag{42}$$

$$\overline{P}_{U_1} = \frac{K_1 \mathrm{e}^{-\frac{\varphi}{2}}}{2\pi} \sum_{i=1}^{2} \left[\sum_{m=0}^{\infty} \sum_{g=0}^{\infty} \frac{\eta_{1,i}\Gamma(m+1)\left(\frac{\varphi\epsilon_{1,i}}{4\mu_{1,i}}\right)^{\frac{m}{2}} g!}{\Gamma(m+1+g)^2} \left[\frac{\Gamma\left(1+\frac{m}{2}+g\right)}{\Gamma\left(1+\frac{m}{2}\right)} \times \frac{\Gamma\left(\frac{m}{2}+\frac{1}{2}+g\right)}{\Gamma\left(\frac{m}{2}+\frac{1}{2}\right)} \right] \epsilon_{1,i}^{g} \times \int_0^{\frac{\pi}{2}} \left(\xi_{1,i}\left(\mu_{1,i}\right)\right)^{g+1} d\phi_{1,i} \right]$$
$$= \frac{K_1 \mathrm{e}^{-\frac{\varphi}{2}}}{\sqrt{\pi}} \sum_{i=1}^{2} \left[\left[\sum_{m=0}^{\infty} \sum_{g=0}^{\infty} \frac{\eta_{1,i}\left(\frac{\epsilon_{1,i}\varphi}{4\mu_{1,i}}\right)^{\frac{m}{2}} \left(\frac{\epsilon_{1,i}}{2}\right)^{g} \left(\frac{m}{2}+g\right)\Gamma(m+2g)}{\left(\Gamma(g+1)\Gamma(m+g+1)\right)^2} \right] \times \left(\frac{-2{}_2F_1\left(\left[\frac{1}{2}, \frac{3}{2}+g\right], \left[\frac{3}{2}\right], -\frac{1}{2\mu_{1,i}}\right)\Gamma\left(\frac{3}{2}+g\right)}{\left(2\mu_{1,i}\right)^{g+\frac{3}{2}}} + \frac{\sqrt{\pi}\Gamma(g+1)}{\left(2\mu_{1,i}\right)^{g+1}} \right) \right] \tag{44}$$

${}_2F_1([t_1, t_2, ...t_p]; [A_1, A_2, ..., g_q]; J)$ is the generalized hypergeometric function which can be represented by the following infinite series [48]

$${}_2F_1([t_1, t_2, ...t_p]; [A_1, A_2, ..., A_q]; J) = \sum_{g=0}^{\infty} \frac{J^g \prod_{l=1}^{p} \frac{\Gamma(t_l+g)}{\Gamma(t_l)}}{\prod_{L=1}^{q} \frac{\Gamma\left(A_L+g\right)}{\Gamma\left(A_L\right)}}. \tag{43}$$

Then, by replacing the generalized hypergeometric function by its series expansion, the average BER for the first user can be expressed as in (44), shown at the top of this page.

In order to evaluate the average BER for the second user, both (24) and (37) are used as given in (45) at the bottom of this page. Now, the term $\overline{P}^1_{U_2}$ can be computed as

$$\overline{P}^1_{U_2} = K_2\eta_{2,i} \int_0^{\infty} Q\left(\sqrt{\gamma_{2,i}}\right) \mathrm{e}^{-\frac{\mu_{2,i}\gamma_{2,i}}{2}} I_0\left(\sqrt{\epsilon_{2,i}\gamma_{2,i}}\right) d\gamma_{2,i}. \tag{46}$$

By using the integral representation of the Q function

$$\overline{P}^1_{U_2} = \frac{K_2\eta_{2,i}}{\pi} \int_0^{\frac{\pi}{2}} \int_0^{\infty} \mathrm{e}^{-\frac{2\gamma_{2,i}}{\xi_{2,i}\left(\mu_{2,i}\right)}} \times I_0\left(\sqrt{\epsilon_{2,i}\gamma_{2,i}}\right) d\gamma_{2,i} d\phi_{2,i}. \tag{47}$$

The evaluation of the inner integral in (47) is given as [45]

$$\overline{P}^1_{U_2} = \frac{K_2\eta_{2,i}}{\pi} \int_0^{\frac{\pi}{2}} \xi_{2,i}\left(\mu_{2,i}\right) \mathrm{e}^{\frac{\xi_{2,i}\left(\frac{\mu_{2,i}}{2}\right)\epsilon_{2,i}}{4}} d\phi_{2,i}. \tag{48}$$

The integral in (48) is analytically intractable; hence, the following series representation for e^x is utilized:

$$\mathrm{e}^x = \sum_{z=0}^{\infty} \frac{x^z}{z!} = 1 + x + \frac{x^2}{2} + \frac{x^3}{6} + \frac{x^4}{24}. \tag{49}$$

Then

$$\overline{P}^1_{U_2} = \frac{K_2\eta_{2,i}}{\pi} \sum_{z=0}^{\infty} \frac{1}{z!} \left(\frac{\epsilon_{2,i}}{4}\right)^z \int_0^{\frac{\pi}{2}} \left(\xi_{2,i}\left(\frac{\mu_{2,i}}{2}\right)\right)^{z+1} d\phi_{2,i}. \tag{50}$$

$$\overline{P}_{U_2} = \frac{1}{2} \sum_{i=1}^{5} v_i \left[\int_0^{\infty} Q\left(\sqrt{\gamma_{2,i}}\right) f_2\left(\gamma_{2,i}\right) d\gamma_{2,i} \right], \mathbf{v} = [2, -1, 1, 1, -1]$$
$$= \frac{K_2}{2} \sum_{i=1}^{5} v_i \left[\int_0^{\infty} Q\left(\sqrt{\gamma_{2,i}}\right) \eta_{2,i} \mathrm{e}^{-\frac{\mu_{2,i}\gamma_{2,i}}{2}} I_0\left(\sqrt{\epsilon_{2,i}\gamma_{2,i}}\right) d\gamma_{2,i} - \mathrm{e}^{-\frac{\varphi}{2}} \int_0^{\infty} Q\left(\sqrt{\gamma_{2,i}}\right) \eta_{2,i} I_0\left(\sqrt{\epsilon_{2,i}\gamma_{2,i}}\right) \mathrm{e}^{-\gamma_{2,i}\mu_{2,i}} \times \sum_{m=0}^{\infty} \left(\frac{\varphi}{\mu_{2,i}\gamma_{2,i}}\right)^{\frac{m}{2}} I_m\left(\sqrt{\epsilon_{2,i}\gamma_{2,i}}\right) d\gamma_{2,i} \right]$$
$$= \frac{1}{2} \sum_{i=1}^{5} v_i \left[\overline{P}^1_{U_2} - \overline{P}^2_{U_2} \right] \tag{45}$$

$$\overline{P}_{U_2} = \frac{K_2}{2\sqrt{\pi}} \sum_{i=1}^{5} \left[\eta_{2,i} \sum_{z=0}^{\infty} \frac{\left(\frac{\epsilon_{2,i}}{2\mu_{2,i}}\right)^z}{z!} \left(\frac{-2_2F_1\left(\left[\frac{1}{2}, \frac{3}{2}+z\right], \left[\frac{3}{2}\right], \frac{-1}{2}\right)\Gamma\left(\frac{3}{2}+z\right)}{\mu_{2,i}^{\frac{3}{2}}\Gamma(z+1)} + \sqrt{\frac{\pi}{\mu_{2,i}^2}} \right) - \frac{2K_2\eta_{2,i}\mathrm{e}^{-\frac{\varphi}{2}}}{\sqrt{\pi}} \times \right.$$

$$\left. \sum_{m=0}^{\infty}\sum_{g=0}^{\infty} \frac{\left(\frac{\epsilon_{2,i}\varphi}{4\mu_{2,i}}\right)^{\frac{m}{2}} \left(\frac{\epsilon_{2,i}}{2}\right)^g \left(\frac{m}{2}+g\right)\Gamma(m+2g)}{\left(\Gamma(g+1)\Gamma(m+g+1)\right)^2} \left(\frac{-2_2F_1\left(\left[\frac{1}{2}, \frac{3}{2}+g\right], \left[\frac{3}{2}\right], -\frac{1}{2\mu_{2,i}}\right)\Gamma\left(\frac{3}{2}+g\right)}{\left(2\mu_{2,i}\right)^{g+\frac{3}{2}}} + \frac{\sqrt{\pi}\Gamma(g+1)}{\left(2\mu_{2,i}\right)^{g+1}} \right) \right]$$

$$\mathbf{v} = [2, -1, 1, 1, -1] \tag{52}$$

Evaluating the integral gives

$$\overline{P}_{U_2}^{1} = \frac{K_2\eta_{2,i}}{\sqrt{\pi}} \sum_{z=0}^{\infty} \frac{1}{z!} \left(\frac{\epsilon_{2,i}}{2\mu_{2,i}}\right)^z \times \left(\frac{-2_2F_1\left(\left[\frac{1}{2}, \frac{3}{2}+z\right], \left[\frac{3}{2}\right], \frac{-1}{2}\right)}{\mu_{2,i}^{\frac{3}{2}}\Gamma(z+1)\Gamma^{-1}\left(\frac{3}{2}+z\right)} + \sqrt{\frac{\pi}{\mu_{2,i}^2}} \right). \tag{51}$$

The second term $\overline{P}_{U_2}^{2}$ in (45) can be computed by following the approach of $\overline{P}_{U_1}$. As a result, the total average BER for the second user can be represented as in (52) given at the top of this page.

REFERENCES

[1] S. Sekander, H. Tabassum, and E. Hossain, "Multi-tier drone architecture for 5G/B5G cellular networks: Challenges, trends, and prospects," *IEEE Commun. Mag.*, vol. 56, no. 3, pp. 96–103, Mar. 2018.

[2] M. Jia, X. Gu, Q. Guo, W. Xiang, and N. Zhang, "Broadband hybrid satellite-terrestrial communication systems based on cognitive radio toward 5G," *IEEE Wireless Commun.*, vol. 23, no. 6, pp. 96–106, Dec. 2016.

[3] M. A. Al-Jarrah, M. A. Yaseen, A. Al-Dweik, O. A. Dobre, and E. Alsusa, "Decision fusion for IoT-based wireless sensor networks," *IEEE Internet Things J.*, vol. 7, no. 2, pp. 1313–1326, Feb. 2020.

[4] Y. Iraqi and A. Al-Dweik, "Adaptive bit loading with reduced computational time and complexity for multicarrier wireless communications," *IEEE Trans. Aerosp. Electron. Syst.*, vol. 56, no. 3, pp. 2497–2506, Jun. 2020.

[5] J. Tooker and M. C. Vuran, "Mobile data harvesting in wireless underground sensor networks," in *Proc. SECON*, Jun. 2012, pp. 560–568.

[6] H. Mukhtar *et al.*, "Adaptive hybrid ARQ system using turbo product codes with hard/soft decoding," *IEEE Commun. Lett.*, vol. 17, no. 11, pp. 2132–2135, Nov. 2013.

[7] H. Mukhtar, A. Al-Dweik, and M. Al-Mualla, "Low complexity power optimization algorithm for multimedia transmission over wireless networks," *IEEE J. Sel. Top. Signal Process.*, vol. 9, no. 1, pp. 113–124, Feb. 2015.

[8] C. Deng, M. Liu, X. Li, and Y. Liu, "Hardware impairments aware full-duplex NOMA networks over Rician fading channels," *IEEE Syst. J.*, vol. 15, no. 2, pp. 2515–2518, Jun. 2021.

[9] T. Assaf, A. Al-Dweik, M. E. Moursi, and H. Zeineldin, "Exact BER performance analysis for downlink NOMA systems over Nakagami- m fading channels," *IEEE Access*, vol. 7, pp. 134539–134555, 2019.

[10] D. Hu, Q. Zhang, Q. Li, and J. Qin, "Joint position, decoding order, and power allocation optimization in UAV-based NOMA downlink communications," *IEEE Syst. J.*, vol. 14, no. 2, pp. 2949–2960, Jun. 2020.

[11] Q. He, Y. Hu, and A. Schmeink, "Closed-form symbol error rate expressions for non-orthogonal multiple access systems," *IEEE Trans. Veh. Technol.*, vol. 68, no. 7, pp. 6775–6789, Jul. 2019.

[12] X. Yan, H. Xiao, K. An, G. Zheng, and S. Chatzinotas, "Ergodic capacity of NOMA-based uplink satellite networks with randomly deployed users," *IEEE Syst. J.*, vol. 14, no. 3, pp. 3343–3350, Sep. 2020.

[13] M. Zeng, A. Yadav, O. A. Dobre, G. I. Tsiropoulos, and H. V. Poor, "Capacity comparison between MIMO-NOMA and MIMO-OMA with multiple users in a cluster," *IEEE J. Sel. Areas Commun.*, vol. 35, no. 10, pp. 2413–2424, Oct. 2017.

[14] F. Kara and H. Kaya, "On the error performance of cooperative-NOMA with statistical CSIT," *IEEE Commun. Lett.*, vol. 23, no. 1, pp. 128–131, Jan. 2019.

[15] M. Tian, S. Zhao, Q. Li, and J. Qin, "Secrecy sum rate optimization in nonorthogonal multiple access AF relay networks," *IEEE Syst. J.*, vol. 13, no. 3, pp. 2712–2715, Sep. 2019.

[16] F. Kara and H. Kaya, "BER performances of downlink and uplink NOMA in the presence of SIC errors over fading channels," *IET Commun.*, vol. 12, no. 15, pp. 1834–1844, Sep. 2018.

[17] S. K. Zaidi, S. F. Hasan, and X. Gui, "Evaluating the Ergodic rate in SWIPT-aided hybrid NOMA," *IEEE Commun. Lett.*, vol. 22, no. 9, pp. 1870–1873, Sep. 2018.

[18] L. Bariah, S. Muhaidat, and A. Al-Dweik, "Error probability analysis of non-orthogonal multiple access over Nakagami-m fading channels," *IEEE Trans. Commun.*, vol. 67, no. 2, pp. 1586–1599, Feb. 2019.

[19] C. Xu, M. Wu, Y. Xu, and Y. Fang, "Uplink low-power scheduling for delay-bounded industrial wireless networks based on imperfect power-domain NOMA," *IEEE Syst. J.*, vol. 14, no. 2, pp. 2443–2454, Jun. 2020.

[20] X. Wang, M. Jia, Q. Guo, I. W. Ho, and F. C. Lau, "Full-duplex relaying cognitive radio network with cooperative nonorthogonal multiple access," *IEEE Syst. J.*, vol. 13, no. 4, pp. 3897–3908, Dec. 2019.

[21] L. Dai, B. Wang, Z. Ding, Z. Wang, S. Chen, and L. Hanzo, "A survey of non-orthogonal multiple access for 5G," *IEEE Commun. Surv. Tut.*, vol. 20, no. 3, pp. 2294–2323, May 2018.

[22] M. Al-Imari, M. A. Imran, R. Tafazolli, and D. Chen, "Subcarrier and power allocation for LDS-OFDM system," in *Proc. IEEE VTC-Spring*, May 2011, pp. 1–5.

[23] S. M. R. Islam, N. Avazov, O. A. Dobre, and K. Kwak, "Power-domain non-orthogonal multiple access (NOMA) in 5G systems: Potentials and challenges," *IEEE Commun. Surv. Tut.*, vol. 19, no. 2, pp. 721–742, Oct. 2017.

[24] J. Ding, J. Cai, and C. Yi, "An improved coalition game approach for MIMO-NOMA clustering integrating beamforming and power allocation," *IEEE Trans. Veh. Technol.*, vol. 68, no. 2, pp. 1672–1687, Feb. 2019.

[25] M. S. Ali, E. Hossain, A. Al-Dweik, and D. I. Kim, "Downlink power allocation for CoMP-NOMA in multi-cell networks," *IEEE Trans. Commun.*, vol. 66, no. 9, pp. 3982–3998, Sep. 2018.

[26] J. Garnier, A. Fabre, H. Fares, and R. Bonnefoi, "On the performance of QPSK modulation over downlink NOMA: From error probability derivation to SDR-based validation," *IEEE Access*, vol. 8, pp. 66495–66507, 2020.

[27] F. Kara and H. Kaya, "Error probability analysis of NOMA-based diamond relaying network," *IEEE Trans. Veh. Technol.*, vol. 69, no. 2, pp. 2280–2285, Feb. 2020.

[28] Z. Gao, A. Liu, and X. Liang, "The performance analysis of downlink NOMA in LEO satellite communication system," *IEEE Access*, vol. 8, pp. 93723–93732, 2020.

[29] B. K. Ng and C. Lam, "Joint power and modulation optimization in two-user non-orthogonal multiple access channels: A minimum error probability approach," *IEEE Trans. Veh. Technol.*, vol. 67, no. 11, pp. 10693–10703, Nov. 2018.

[30] C. Yan, A. Harada, A. Benjebbour, Y. Lan, A. Li, and H. Jiang, "Receiver design for downlink non-orthogonal multiple access (NOMA)," in *Proc. IEEE VTC-Spring*, May 2015, pp. 1–6.

[31] M. Qiu, Y. Huang, S. Shieh, and J. Yuan, "A lattice-partition framework of downlink non-orthogonal multiple access without SIC," *IEEE Trans. Commun.*, vol. 66, no. 6, pp. 2532–2546, Jun. 2018.

[32] S. Shieh, C. Lin, Y. Huang, and C. Wang, "On gray labeling for downlink non-orthogonal multiple access without SIC," *IEEE Commun. Lett.*, vol. 20, no. 9, pp. 1721–1724, Sep. 2016.

[33] J. S. Yeom, H. S. Jang, K. S. Ko, and B. C. Jung, "BER performance of uplink NOMA with joint maximum-likelihood detector," *IEEE Trans. Veh. Technol.*, vol. 68, no. 10, pp. 10295–10300, Aug. 2019.

[34] S. Baig, U. Ali, H. M. Asif, A. A. Khan, and S. Mumtaz, "Closed-form BER expression for Fourier and wavelet transform-based pulse-shaped data in downlink NOMA," *IEEE Commun. Lett.*, vol. 23, no. 4, pp. 592–595, Apr. 2019.

[35] F. Kara and H. Kaya, "Performance analysis of SSK-NOMA," *IEEE Trans. Veh. Technol.*, vol. 68, no. 7, pp. 6231–6242, Jul. 2019.
[36] R. Sun and D. W. Matolak, "Air-ground channel characterization for unmanned aircraft systems part II: Hilly and mountainous settings," *IEEE Trans. Veh. Technol.*, vol. 66, no. 3, pp. 1913–1925, Mar. 2017.
[37] D. W. Matolak and R. Sun, "Air-ground channel characterization for unmanned aircraft systems-part III: The suburban and near-urban environments," *IEEE Trans. Veh. Technol.*, vol. 66, no. 8, pp. 6607–6618, Aug. 2017.
[38] M. Banagar, H. S. Dhillon, and A. F. Molisch, "Impact of UAV wobbling on the air-to-ground wireless channel," *IEEE Trans. Veh. Technol.*, vol. 69, no. 11, pp. 14025–14030, Nov. 2020.
[39] T. Assaf, A. Al-Dweik, M. S. El Moursi, H. Zeineldin, and M. Al-Jarrah, "Exact bit error-rate analysis of two-user NOMA using QAM with arbitrary modulation orders," *IEEE Commun. Lett.*, vol. 24, no. 12, pp. 2705–2709, Dec. 2020.
[40] M. Tariq, A. Al-Dweik, B. Mohammad, H. Saleh, and T. Stouraitis, "Computational power evaluation for energy-constrained wireless communications systems," *IEEE Open J. Commun. Soc.*, vol. 1, pp. 308–319, Mar. 2020.
[41] F. Kara and H. Kaya, "Error probability analysis of non-orthogonal multiple access with channel estimation errors," in *Proc. IEEE Int. Black Sea Conf. Commun. Netw. (BlackSeaCom)*, Odessa, Ukraine, May 2020, pp. 1–5, doi: 10.1109/BlackSeaCom48709.2020.9234956.
[42] F. Kara and H. Kaya, "Improved user fairness in decode-forward relaying non-orthogonal multiple access schemes with imperfect SIC and CSI," *IEEE Access*, vol. 8, pp. 97540–97556, 2020.
[43] M. Mirahmadi, A. Al-Dweik, and A. Shami, "Interference modeling and performance evaluation of heterogeneous cellular networks," *IEEE Trans. Commun.*, vol. 62, no. 6, pp. 2132–2144, Jun. 2014.
[44] D. Anirban, "Finite sample theory of order statistics and extremes," in, *Probability for Statistics and Machine Learning: Fundamentals and Advanced Topics*. Berlin, Germany: Springer, 2011.
[45] I. Gradshteyn and I. Ryzhik, *Table of Integrals, Series, and Products*, 7th ed. New York, NY, USA: Academic, 2007.
[46] M. Simon and M. Alouini, *Digital Communication over Fading Channels*. Hoboken, NJ, USA: Wiley, Jan. 2000.
[47] J. Craig, "A new, simple and exact result for calculating the probability of error for two-dimensional signal constellations," in *Proc. MILCOM91*, Nov. 1991, pp. 571–575.
[48] G. Gasper and M. Rahman, *Encyclopedia of Mathematics and Its Applications* (Basic Hypergeometric Series 96), 2nd ed. Cambridge, U.K.: Cambridge Univ. Press, 2004.

Tasneem Assaf (Student Member, IEEE) received the B.Sc. degree in communications engineering from Khalifa University, Abu Dhabi, UAE, in 2014, and the master's degree in electrical engineering from the American University of Sharjah, Sharjah, UAE, in 2016. She is currently working toward the Ph.D. degree in electrical and computer engineering at Khalifa University.

Her research interests include smart grids, optimization, wireless communications, and machine learning.

Arafat Al-Dweik (Senior Member, IEEE) received the M.S. (*Summa Cum Laude*) and Ph.D. (*Magna Cum Laude*) degrees in electrical engineering from Cleveland State University, Cleveland, OH, USA, in 1998 and 2001, respectively.

He was with Efficient Channel Coding, Inc., Cleveland, OH, USA, from 1999 to 2001. From 2001 to 2003, he was the Head of Department of Information Technology, Arab American University, Jenin, Palestine. Since 2003, he has been with the Department of Electrical Engineering, Khalifa University, Abu Dhabi, United Arab Emirates. He was with University of Guelph, ON, Canada, as an Associate Professor from 2013 to 2014. He is a Visiting Research Fellow with the School of Electrical, Electronic, and Computer Engineering, Newcastle University, Newcastle upon Tyne, U.K, and a Research Professor with Western University, London, ON, Canada, and University of Guelph, Guelph, Canada. He has extensive research experience in various areas of wireless communications that include modulation techniques, channel modeling and characterization, synchronization and channel estimation techniques, OFDM technology, error detection and correction techniques, MIMO, and resource allocation for wireless networks.

Dr Al-Dweik has extensive editorial experience and he has served as an Associate Editor for the IEEE TRANSACTIONS ON VEHICULAR TECHNOLOGY and the *IET Communications*. He is a member of Tau Beta Pi and Eta Kappa Nu. He was awarded the Fulbright scholarship from 1997 to 1999. He was the recipient of the Hijjawi Award for Applied Sciences in 2003, the Fulbright Alumni Development Grant in 2003 and 2005, and the Dubai Award for Sustainable Transportation in 2016. He is a Registered Professional Engineer in the Province of Ontario, Canada.

Mohamed S. El Moursi (Senior Member, IEEE) received the B.Sc. and M.Sc. degrees from Mansoura University, Mansoura, Egypt, in 1997 and 2002, respectively, and the Ph.D. degree from the University of New Brunswick, Fredericton, NB, Canada, in 2005, all in electrical engineering.

He was a Research and Teaching Assistant with the Department of Electrical and Computer Engineering, UNB, from 2002 to 2005. He joined McGill University as a Postdoctoral Fellow with the Power Electronics Group. He joined Vestas Wind Systems, Arhus, Denmark, in the Technology R&D with the Wind Power Plant Group. He was with TRANSCO, UAE, as a Senior Study and Planning Engineer. He is currently a Professor with the Electrical and Computer Engineering Department, Khalifa University of Science and Technology—Masdar Campus, Abu Dhabi, UAE, and seconded to a Professor position with the Faculty of Engineering, Mansoura University, currently on leave. He was a Visiting Professor with Massachusetts Institute of Technology, Cambridge, MA, USA. His research interests include power system, power electronics, FACTS technologies, VSC-HVdc systems, microgrid operation and control, and renewable energy systems (wind and PV) integration and interconnections.

Dr. Shawky is currently an Editor of IEEE TRANSACTIONS ON POWER DELIVERY and IEEE TRANSACTIONS ON POWER SYSTEMS, Associate Editor of IEEE TRANSACTIONS ON POWER ELECTRONICS, Guest Editor of IEEE TRANSACTIONS ON ENERGY CONVERSION, Guest Editor-in-Chief for special section between IEEE TRANSACTIONS ON POWER DELIVERY and IEEE TRANSACTIONS ON POWER SYSTEMS, Editor for IEEE POWER ENGINEERING LETTERS, Regional Editor for *IET Renewable Power Generation*, and Associate Editor for *IET Power Electronics Journals*.

Hatem Zeineldin (Senior Member, IEEE) received the B.Sc. and M.Sc. degrees in electrical engineering from Cairo University, Giza, Egypt, in 1999 and 2002, respectively, and the Ph.D. degree in electrical and computer engineering from the University of Waterloo, Waterloo, ON, Canada, in 2006.

He was with Smith and Andersen Electrical Engineering, Inc., North York, ON, USA, where he was involved in projects involving distribution system designs, protection, and distributed generation. He was a Visiting Professor with the Massachusetts Institute of Technology, Cambridge, MA, USA. He is currently a Professor with the Khalifa University of Science and Technology, Abu Dhabi, UAE, and is currently on leave from the Faculty of Engineering, Cairo University, Giza, Egypt. His current research interests include distribution system protection, distributed generation, and microgrids.

Dr. Zeineldin is currently an Editor for the IEEE TRANSACTIONS ON ENERGY CONVERSION and the IEEE TRANSACTIONS ON SMART GRID.

Mohammad Al-Jarrah (Member, IEEE) received the B.Sc. and M.S. degrees in electrical engineering/wireless communications from Jordan University of Science and Technology (JUST), Irbid, Jordan, in 2011. He is currently working toward the Ph.D. degree in electrical and electronics engineering with the Department of Electrical and Electronic Engineering, The University of Manchester, Manchester, U.K.

From 2017 to 2019, he had been working as a Lab Instructor with Khalifa University (KU), Abu Dhabi, United Arab Emirates. Currently, he is a Marie Curie Early Stage Researcher with the Department of Electrical and Electronic Engineering, The University of Manchester. His research interests include distributed decision fusion systems, statistical signal processing, target tracking in wireless sensor networks, RFID communications, cooperative spectrum sensing, free-space optical communications, cooperative communications, and backhauling and cellular planning for 5G cellular networks.